Polarization-induced torque in optical traps

Stephen H. Simpson, David C. Benito, and Simon Hanna*
H. H. Wills Physics Laboratory, University of Bristol, Tyndall Avenue, Bristol BS8 1TL, United Kingdom
(Received 4 May 2007; published 9 October 2007)

In the field of optical trapping and micromanipulation it is well known that linearly polarized Gaussian beams, which possess no inherent angular momentum, can exert an orienting torque on optically or geometrically anisotropic particles. Conservation of angular momentum requires that the application of such a torque be compensated for by an equivalent, and opposite, angular momentum flux in the beam. In the following paper we analyze this effect in terms of both the scattered field, and the mechanical torque experienced by the particle. It is demonstrated that, in general, the scattered field has a complicated form, carrying both spin and orbital angular momentum. However, we show that the variation of torque with rotation angle is identically equal to $A+B\sin(2\alpha+\beta)$ for arbitrarily shaped particles, where A, B, and β are constants and α is the angular displacement of the major axis of the particle from the polarization direction. The scattered field, and the mechanical torque, are seen to reduce to qualitatively distinct forms that depend on the symmetry group of the scattering particle. Our findings are verified and illustrated by a series of numerical calculations of the forces and torques experienced by arbitrarily shaped particles trapped in linearly polarized Gaussian beams.

DOI: 10.1103/PhysRevA.76.043408 PACS number(s): 32.80.Lg, 42.62.−b, 42.25.Fx, 42.25.Ja

I. INTRODUCTION

When a particle, possessing either geometric or optical anisotropy, is contained in a linearly polarized optical trap, it often experiences a torque that restricts its rotation about the beam axis [1]. Controlling the polarization of the beam gives a way of controlling the orientation of the particle. The effect has obvious applications for micromanipulation and orientation of anisotropic particles such as nanorods and birefringent crystallites. There are other potential applications in microrheology [2], and the ability to accurately impose small torques on single molecules greatly enhances studies of DNA manipulation of the sort described in Refs. [3,4].

In this paper, we will evaluate the torques on a range of optically homogeneous, geometrically anisotropic particles contained in axisymmetric, linearly polarized optical traps. We will restrict our discussion to cases where the particles are constrained to rotate in a plane perpendicular to the beam axis. For the most part we will also limit our discussion to incident beams which possess no angular momentum, of which the linearly polarized Gaussian beam is a common example.

In the simplest analysis, we might approximate the torque by that experienced by a point polarizability,

$$\Gamma = \mathbf{p} \times \mathbf{E}, \tag{1}$$

where the polarization $\mathbf{p}$ is related to the applied field by the polarizability tensor $\underline{\underline{\boldsymbol{\alpha}}}$,

$$\mathbf{p} = \underline{\underline{\boldsymbol{\alpha}}}\mathbf{E}. \tag{2}$$

Simple analysis (e.g., as outlined in the Appendix of Ref. [5]) shows that Γ is proportional to $\sin(2\theta)$, where θ is the angle between the induced dipole and the applied field. This simplistic result applies in the quasistatic limit. In the presence of time varying fields, it is assumed that the particle is sufficiently small that the same phase is experienced at all parts, i.e., that the particle dimensions are small compared with the wavelength of the incident light. The questions remains, therefore, as to whether similar behavior should be expected from a general extended particle of arbitrary shape, and further, whether the symmetry of such a particle will affect the magnitude of torque it experiences.

Because of the significance of polarization-induced torque to micromanipulation, the phenomenon has been subjected to a considerable amount of theoretical and experimental investigation [1,4–15]. Experimentally, the induced torque may be evaluated by observing the motion of a particle in a rotating beam of linearly polarized light, given a knowledge of the appropriate hydrodynamic friction tensor [1]. Alternatively, the torque may be estimated from a comparison of the powers in the right and left circularly polarized components of the transmitted beam [12,13], although this method neglects part of the scattered field and can therefore only provide an approximation.

The variety of theoretical approaches that have been used to estimate torques reflects the fact that optical trapping experiments are often carried out at length scales that lie in a region abutted by several different physical regimes. Thus the Rayleigh limit, in which particles are represented by point polarizabilities (see above), has been taken by some authors [5,11] while others rely on the short wavelength limit to perform ray optics calculations [7]. Attempts at incorporating quantum mechanical effects have been made by calculating momentum transfer from photon flux calculations [10]. In the classical regime, however, a completely rigorous calculation would consist of a solution of Maxwell's equations for the total electromagnetic field, followed by a calculation of the rate at which the angular momentum in the total field is changing.

A large number of methods for the solution of the scattering problem exist. As far as the calculations of polarization-induced torque are concerned, the principal candidates are the T-matrix approach [8,9,15–17] and the multiple multipole method [14]. Each of these methods have limitations, of

*S.Hanna@bristol.ac.uk

a pragmatic rather than fundamental sort; in Ref. [14] the calculations are confined to two-dimensional (2D) systems for reasons of computational expense while evaluation of T matrices for arbitrarily shaped particles may be problematic particularly when they are not convex [16].

Having found the total fields surrounding the particle, the torque follows from a consideration of the rate of change of angular momentum in those fields,

$$\frac{\partial \mathcal{L}}{\partial t} = \frac{\partial}{\partial t}\int_V \epsilon\mu[\mathbf{r} \times (\mathbf{E} \times \mathbf{H})]dV. \tag{3}$$

By Newton's third law, this is equal and opposite to the torque on the particle, which may be written as a surface integral of the associated angular momentum flux,

$$\Gamma = -\int_S r\mathrm{d}\mathbf{S} \cdot [\langle \underline{\underline{\mathbf{T}}}_{\mathrm{M}}(\mathbf{r})\rangle \times \hat{\mathbf{r}}]. \tag{4}$$

In Eq. (4), the integration is taken over a sphere of radius r, with its surface in the far-field. $\underline{\underline{\mathbf{T}}}_{\mathrm{M}}$ is the Maxwell stress tensor given by Eq. (5),

$$\langle \underline{\underline{\mathbf{T}}}_{\mathrm{M}}(\mathbf{r})\rangle = \frac{1}{2}\,\mathrm{Re}\left[\epsilon\mathbf{E}(\mathbf{r}) \otimes \mathbf{E}^*(\mathbf{r}) + \mu\mathbf{H}(\mathbf{r}) \otimes \mathbf{H}^*(\mathbf{r}) - \frac{1}{2}(\epsilon|\mathbf{E}(\mathbf{r})|^2 + \mu|\mathbf{H}(\mathbf{r})|^2)\underline{\underline{\mathbf{I}}}\right]. \tag{5}$$

In the above equations, the double underline indicates a second rank tensor, angle brackets denote a time average over a cycle for harmonic fields, the asterisks denote complex conjugates, and the $\otimes$ symbol denotes a dyadic product. $\underline{\underline{\mathbf{I}}}$ is the unit tensor, all of the fields involved in the above equations are total fields, and the material parameters are those of the medium in which the particle is immersed.

In this paper we are principally interested in polarization-induced torque in beams with axisymmetric irradiance distributions, and how it varies with axial rotation. Although the effect may apply equally to geometric or optically anisotropic particles, we will limit ourselves here to an analysis of the geometric case. We will also constrain the discussion to rotations occurring in a plane perpendicular to the beam axis. It is found that a convenient platform for the analysis of this problem is provided by transition matrix (or T matrix) theory. The use of the T-matrix method allows the integral appearing in Eq. (4) to be evaluated analytically using formulas derived by Barton *et al.* [6] (see below, Sec. II A).

We use the T-matrix formalism to investigate, analytically, the interaction of linearly polarized beams with a variety of particles. By examining a series of particles of distinct symmetry, the relationship between the scattered field and induced torque will be elucidated. In doing so, it will be observed that the expression derived by approximating the particle by a point polarizability, while not universally applicable, is valid for a range of extended particles. The expressions obtained apply equally well to any linearly polarized beam whose irradiance and phase possess circular symmetry about the beam axis or propagation direction. Linearly polarized Gaussian beams and plane waves are particular examples of these; higher order beams will be considered in Sec. III D.

The validity of the results obtained is demonstrated computationally. To this end the finite-difference time-domain (FDTD) approach has been chosen for the calculation of the necessary fields. This method involves a direct integration of Maxwell's equations in the time domain and is easily adapted to calculating optically induced torques in the process. The FDTD approach has no underlying assumptions, and so provides an independent verification of the results predicted by the T-matrix method,

In the following sections the T-matrix formalism and the FDTD method are described, after which a systematic study of torques on particles belonging to each of the 2D point symmetry groups is presented.

II. METHODS

A. *T*-matrix theory

The general approach employed by T-matrix theory typifies a range of techniques used in solving linear partial differential equations. Expansions in a complete set of eigenfunctions are used to represent the solution, and any inhomogeneous terms appearing in the equation. Unknown expansion coefficients are subsequently sought by applying boundary conditions. In the case of light scattering calculations the linearity of the scattering process leads to linear relationships between the coefficients of the incident field expansion and those of the scattered field.

T-matrix theory is extensively discussed elsewhere (see [16], for example); for now it suffices to state the axioms that underpin it. They are as follows: (i) The incident field can be expanded, about a fixed point, in a set of "regularized" vector spherical wave functions (VSWFs),

$$\mathbf{E}^{\mathrm{inc}}(\mathbf{r}) = \sum_{n=1}^{\infty}\sum_{m=-n}^{n}[a_{nm}^{(1)}\mathcal{R}\mathbf{M}_{nm}(k_1\mathbf{r}) + a_{nm}^{(2)}\mathcal{R}\mathbf{N}_{nm}(k_1\mathbf{r})]. \tag{6}$$

(ii) The scattered field can be expanded in an "unregularized" set of VSWFs,

$$\mathbf{E}^{\mathrm{sca}}(\mathbf{r}) = \sum_{n=1}^{\infty}\sum_{m=-n}^{n}[p_{nm}^{(1)}\mathbf{M}_{nm}(k_1\mathbf{r}) + p_{nm}^{(2)}\mathbf{N}_{nm}(k_1\mathbf{r})]. \tag{7}$$

(iii) The coefficients appearing in the incident field expansion are linearly related to the coefficients in the scattered field expansion by the T matrix,

$$\tilde{p} = T\tilde{a}, \tag{8}$$

where $\tilde{a}$ is a vector constructed from an ordered list of incident beam expansion coefficients,

$$\tilde{a} = (a_{1,-1}^{(1)}, a_{1,0}^{(1)}, a_{1,1}^{(1)}, a_{2,-2}^{(1)}, a_{2,-1}^{(1)}, \ldots, a_{\infty,\infty}^{(1)}, a_{1,-1}^{(2)}, a_{1,0}^{(2)}, a_{1,1}^{(2)}, a_{2,-2}^{(2)}, a_{2,-1}^{(2)}, \ldots, a_{\infty,\infty}^{(2)}). \tag{9}$$

A similar definition applies for the scattered beam coefficients, $\tilde{p}$. k_1 represents the wave vector of the beam incident field in the background medium, and the transition (or "T")

matrix depends on the geometry and optical properties of the particle of interest, and is to be determined. Expansions for the incident and scattered magnetic fields $\mathbf{H}^{\mathrm{inc}}$ and $\mathbf{H}^{\mathrm{sca}}$ may be obtained from Eqs. (6) and (7) by multiplying by the scalar quantity $i\sqrt{\epsilon/\mu}$, and placing the expansion coefficients with superscript (2) before those with the superscript (1) in $\tilde{a}$.

The VSWFs, $\mathbf{M}_{nm}$, $\mathbf{N}_{nm}$, $\mathcal{R}\mathbf{M}_{nm}$, and $\mathcal{R}\mathbf{N}_{nm}$ are a complete set of orthogonal solutions to the vector Helmholtz equation [18]. The individual functions are labeled by two indices m and n, the former dictating the azimuthal dependence $[\exp(im\phi)]$ while a combination of the two specify the associated Legendre functions appearing in the polar variation. In the regularized functions, the radial dependence is represented by spherical Bessel functions of order n, whereas spherical Hankel functions appear in the unregularized functions. The special feature of the regularized functions is that they are finite at the origin. The VSWFs appearing in Eqs. (6) and (7) are identical to those described in Ref. [19] apart from a normalizing factor.

Given a T matrix for the particle being considered, Eq. (8) effectively solves the scattering problem. Equations (6) and (7) can subsequently be used to evaluate the total field thereby enabling the computation of the torque by Eq. (4). The integration can be performed analytically, leading to the equations given in Refs. [6,15]. In particular, in terms of the basis set used here, the z component of the torque is given by

$$\Gamma_z = -\frac{\epsilon_{\mathrm{ext}}}{2\pi k_1^3}\sum_{k=1}^{2}\sum_{n=1}^{\infty}\sum_{m=-n}^{n} m[|p_{nm}^{(k)}|^2 + \mathrm{Re}(p_{nm}^{(k)} a_{nm}^{*(k)})]. \quad (10)$$

This expression will be used as the basis of the theoretical results presented below (Sec. III).

B. The FDTD method

The finite-difference time-domain method (FDTD) is a well-known numerical scheme for integrating Maxwell's curl equations on a lattice in the time domain [20,21]. It has been applied to optical trapping by a number of previous workers (see, e.g., [22–24]). Our implementation is a full 3D solution to the scattering problem. It uses a "uniaxial perfectly matched layer" (UPML) [25] to truncate the simulation region in such a way as to mimic an infinite, empty space surrounding the simulated region. In addition the code is parallelized according to a simple domain decomposition, and runs on a 40 processor computing cluster. The beam is injected into the simulation by applying appropriate equivalent electric and magnetic currents. If the desired incident electric field is $\mathbf{E}^{\mathrm{inc}}$ and the magnetic counterpart $\mathbf{H}^{\mathrm{inc}}$ then, by the field equivalence theorem [20,26], these fields can be thought of as deriving from the following equivalent currents:

$$\mathbf{J}^{\mathrm{inc}} = \mathbf{n} \times \mathbf{H}^{\mathrm{inc}}, \quad (11a)$$

$$\mathbf{M}^{\mathrm{inc}} = -\mathbf{n} \times \mathbf{E}^{\mathrm{inc}}, \quad (11b)$$

where $\mathbf{n}$ is the unit normal to the surface on which the currents are imposed. The functions $\mathbf{E}^{\mathrm{inc}}$ and $\mathbf{H}^{\mathrm{inc}}$ need to be independently acquired and generally take the form of frequency domain expressions, in which case time-domain quantities are obtained by multiplying by the appropriate time variation ($e^{i\omega t}$ or $e^{-i\omega t}$, dependent on the adopted convention) and taking the real part.

In the present case, $\mathbf{E}^{\mathrm{inc}}$ and $\mathbf{H}^{\mathrm{inc}}$ derive from a multipole expansion of a fifth-order Davis beam (see below). The resulting currents are evaluated at each time step and added to the appropriate electric and magnetic field components on a horizontal plane covering the entire simulation space (barring the regions occupied by the UPML). Because of the way in which the electric and magnetic field components are interleaved in the FDTD lattice the planes on which the equivalent electric and magnetic currents are applied differ by one half of a cell dimension and this needs to be accounted for when the currents are evaluated. The resulting scheme is similar to the conventional method for injecting plane waves into FDTD lattices with the difference that the field magnitudes and phases have been modified according to the desired incident field.

A recurrent problem in generating appropriate sourcing conditions for beams in any computational electromagnetics solver revolves around the fact that the theory of beam optics has been primarily conducted under the paraxial approximation (i.e., the assumption that the variation of the beam amplitude parallel to the direction of propagation is much slower than other variations). Evidently, this assumption is not appropriate in the vicinity of the focal plane of a beam that is focused at, or near, the diffraction limit. Furthermore, solutions to the paraxial wave equation are intrinsically paradoxical [27]: they are plane polarized but the electric field vector is a function of the transverse distance. Conversely, in the context of the Helmholtz equation the only solutions that satisfy the former condition are plane waves. A focused beam can be thought of as a superposition of plane waves with wave vectors pointing toward the focal region and the component of the electric field vector parallel to the beam axis, $\mathbf{E}_z$, will generally be nonzero. These two considerations imply that, in the present situation, solutions to the paraxial equation are not the most suitable choice of fields with which to generate the equivalent currents $\mathbf{J}^{\mathrm{inc}}$ and $\mathbf{M}^{\mathrm{inc}}$.

The most conspicuous artifact introduced by reliance on the solution to the paraxial wave equation is overestimation of wave front curvature in the vicinity of the beam focus. The effect is to introduce asymmetry along the beam axis, with the intensity profile of the beam flattened above the focus, and distended below (see Fig. 1, dashed line). The problem arises because the paraxial modes are solutions of the paraxial wave equation, whereas the FDTD method propagates the electromagnetic field components according to Maxwell's curl equations. We overcome this difficulty by using exact solutions to Maxwell's equations in the form of the multipole expansion for a fifth order Davis beam given in [28]. This multipole expansion is easily manipulated to give magnetic fields enabling the generation of the necessary equivalent currents (see [16], for example). In contrast to the paraxial approximation the intensity profile of the beam derived in this way is reasonably symmetric along the beam axis (see Fig. 1, solid line). Any remaining asymmetry may be attributed to a number of causes including numerical dispersion and the finiteness of the source.

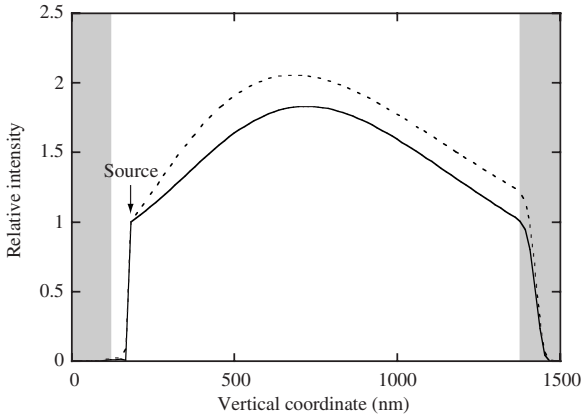

FIG. 1. Longitudinal section showing the intensity along the axis of a focused beam in a FDTD simulation, generated via (a) the paraxial approximation, and (b) a multipole expansion. The position of the source is shown. The gray regions indicate the positions of the absorbing boundary layers.

Having defined the source, the interaction of the beam with an arbitrary particle is achieved simply by assigning the desired electric permittivity to the region of simulation space lying within the particle. The torque experienced by the particle is found by numerically integrating Eq. (4) and averaging over time. Estimated values for the torque are generated at each time step and the simulation is run until convergence has been reached. In the simulations described below, radiation with a frequency of 4.5×10^{14} Hz (wavelength 666 nm) has been used, the background medium is water (with a refractive index of 1.32), and the beam is as described above, with a waist radius of $\lambda/2$. The lattice spacing is 7 nm, unless otherwise specified, and the time step is chosen according to the Courant condition [20,21]. Numerical values of torque are normalized against the beam power [it follows from Eq. (4) that torque is proportional to power] and are quoted in units of pN nm/W.

FDTD calculations are performed on silica particles (refractive index 1.45) of the type shown in Fig. 2 amended in accordance with the quoted symmetry. It should be borne in mind that we are only interested in the axial symmetry of the particle, specifically about the beam axis (z axis). Therefore, we will only consider the two-dimensional point symmetry of the particle, in which the unique axis is parallel to the beam. Thus, the particle shown in Fig. 2(a) has C_1 symmetry with respect to rotations about the (vertical) beam axis. Similarly, Fig. 2(b) shows a particle with C_4 symmetry, i.e., a vertical tetrad axis but no mirror planes, and Fig. 2(c) shows one with D_4 symmetry, i.e., a tetrad with parallel mirrors. A particle with, say, D_3 symmetry will resemble the particle shown in Fig. 2(c) but with three arms instead of four.

Strictly speaking, flat particles of the type shown in Fig. 2 would be expected to twist out of the focal plane, to lie along the beam axis, unless the beam waist is sufficiently large to encompass the whole particle [29]. For the purposes of the present analysis, we will assume that the particles are constrained with their planes perpendicular to the beam axis, in the style of several recent experiments [11,12,30].

For illustrative purposes, Fig. 3 shows a transverse section

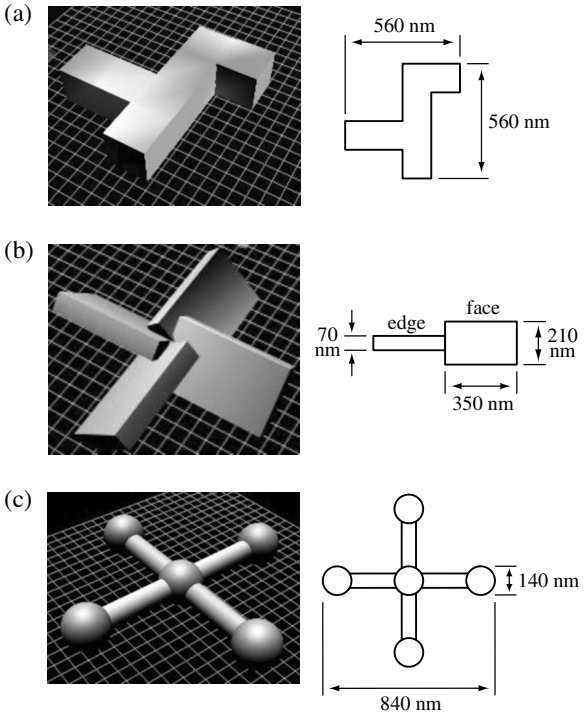

FIG. 2. Illustration of particles with (a) C_1, (b) C_4, and (c) D_4 symmetry about the vertical axis. The dimensions of the particles are indicated: the drawings are to scale.

through a FDTD simulation of a particle with C_1 symmetry, aligned with its plane perpendicular to the beam axis. The z component of the electric field is shown, which is generally nonzero for the reason mentioned above.

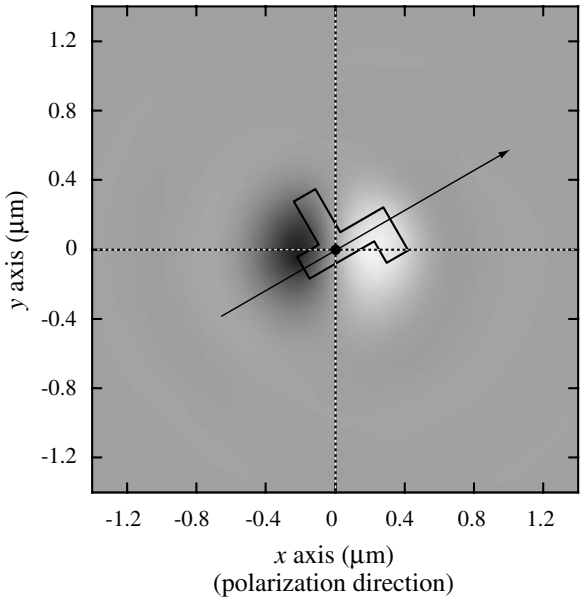

FIG. 3. z component of the electric field near to a C_1 particle, taken from a FDTD simulation of a particle at the focus of an optical trap. The arrow shows the reference axis of the particle, and the spot marks the center of rotation used in subsequent calculations.

III. THEORY AND SIMULATION

A. Introduction

The existence of mechanical torques, in any physical system, is governed by a fundamental symmetry rule. If the system contains a mirror plane, the torque about any axis lying in that plane must be zero. Conversely, when this condition does not pertain, the torque about any axis will be nonzero, except under special circumstances, e.g., a fortuitous cancellation. In the present context, the system consists of a combination of the total (i.e., scattered plus incident) electromagnetic fields and the scattering particle itself. In fact, the symmetry group of the scattered field must be the same as that of the subsystem comprising the incident field and the particle, so only the latter needs to be considered.

In order to apply this principle correctly, it is necessary to be clear about what it means for an electromagnetic field to have a plane of symmetry. This matter is complicated by the fact that the electric field is represented by a polar vector while the magnetic field vector is axial. Consequently, if the electric field is symmetric in a mirror plane the magnetic field will be antisymmetric, as can be verified by considering a symmetric electric field and evaluating the corresponding magnetic field from the appropriate Maxwell's equation ($i\omega\mu\mathbf{H}=\boldsymbol{\nabla}\times\mathbf{E}$). Inspection of Eq. (3) reveals that the significant field symmetry is that of the Poynting vector field, $\mathbf{S}$. If the Poynting vector is invariant with respect to reflection in any plane then the angular momentum density [given by $\mathbf{j}=\epsilon\mu(\mathbf{r}\times\mathbf{S})$] will be odd on reflection in the same plane. Hence, integrating the angular momentum density over all space will give a vector whose components parallel to the symmetry plane will be zero. In other words, if the Poynting vector field contains a symmetry plane, the torque about any axis parallel to this plane will be zero.

In this paper we are solely concerned with rotational behavior about the beam axis, which is here assumed to be coincident with the z or vertical axis of the system. The symmetry condition on the z component of the torque is therefore determined by vertically oriented mirror planes, i.e., mirror planes parallel to the beam axis. Because of this, it is possible to cover all distinct forms of rotational behavior by considering particles chosen from each of the two-dimensional point symmetry groups in turn.

For any specific particle, the induced torque will be related to its angular orientation relative to the polarization direction of the beam in a manner dictated by the angular variation of the products of expansion coefficients appearing in Eq. (10). The T matrix will not generally be diagonal and the azimuthal dependence of the scattered field will differ from that of the incident field. However, this complication does not affect the general form of the relationship between torque and rotation angle, and the details of the particle need not be considered. Adopting this approach leads to a general expression for $\Gamma_z(\alpha)$ that contains a number of unknown constants. Compliance with the previously mentioned symmetry conditions can then be enforced by setting these constants to zero where appropriate.

Although this treatment can account for all of the distinct ways in which these beams can exert mechanical torque, it is not particularly physically illuminating. No insight is gained into the nature of the optical interaction taking place and the symmetry conditions are applied *a priori*; the optical reasons for their manifestation are left obscure. These deficiencies can be rectified by considering the properties of the T matrices of particles belonging to each of the two-dimensional point symmetry groups in turn and by using them to evaluate Eq. (10) in a more explicit manner.

In the following section, the general expression for the variation of optical torque with rotation angle is derived using the simple approach outlined above. Following that, a more complete study is initiated, in which the effect on the T matrix of each of the relevant symmetry groups is considered in turn.

B. Generalized torque expression

For a fifth-order Davis beam, the incident field expansion coefficients have the following form [28]:

$$a_{nm}^{(k)}=\begin{cases} m^{k+1}g_n: & |m|=1, \\ 0: & \text{otherwise}, \end{cases} \tag{12}$$

where g_n, the beam shape coefficients, are complex numbers dependent on the index n. The VSWFs are intrinsically circularly polarized: a linear polarization is constructed from a combination of left- and right-handed circular polarizations represented by $m=\pm 1$. It is worth noting that the two halves of the coefficient vector, $\tilde{a}$, are subject to the following parity condition, which follows from Eq. (12):

$$a_{n1}^{(k)}=(-1)^{k+1}a_{n,-1}^{(k)}. \tag{13}$$

Equations (12) and (13) together determine the direction of polarization of the incident beam; in this case it is parallel to the x axis. It should also be noted that the Poynting vector field of the incident beam contains two vertical mirror planes, one parallel to the direction of polarization, the other orthogonal to it.

Rotations of the incident field can be achieved by applying the rotation theorem for vector spherical wave functions (see the Appendix). For rotations about the z axis this is equivalent to multiplication by the following diagonal matrix:

$$R_{nmn'm'}^{(kk')}(\alpha)=\delta_{kk'}\delta_{nn'}\delta_{mm'}e^{im\alpha}, \tag{14}$$

in which α is the azimuthal angle of rotation. Strictly speaking, Eq. (14) represents a transformation of the VSWFs. However, it may alternatively be interpreted as a transformation of the expansion coefficient vector, $\tilde{a}$. Since the expansion coefficients [Eq. (12)] are only nonzero when $|m|=1$ the rotation matrix can be written in a reduced form,

$$R(\alpha)=\cos(\alpha)I_1+i\sin(\alpha)I_2, \tag{15}$$

where $I_1=\delta_{mm'}\delta_{nn'}\delta_{|m|,1}$ and $I_2=\delta_{mm'}\delta_{nn'}\delta_{|m|,1}m$. This result is specifically only valid for $m=\pm 1$. The rotated incident field coefficients are therefore given by

$$\tilde{a}(\alpha)=\cos(\alpha)I_1\tilde{a}(0)+i\sin(\alpha)I_2\tilde{a}(0), \tag{16}$$

where $\tilde{a}(0)$ represents the unrotated coefficient vector, given by Eq. (12).

Since scalar functions commute with matrices, the multiplication of the T matrix by these incident field coefficients gives the following scattered field coefficients:

$$\tilde{p}(\alpha) = \cos(\alpha) T I_1 \tilde{a}(0) + i \sin(\alpha) T I_2 \tilde{a}(0). \tag{17}$$

The T matrix is not, in general, diagonal. Consequently, the scattered field coefficients, $\tilde{p}$, are not confined to those with values of $|m|=1$ and the azimuthal dependence of the scattered field is more complicated than that of the incident. Nevertheless, comparison of Eqs. (16) and (17) shows that the angular dependence of both sets of coefficients have the same general form, i.e.,

$$a(\alpha) = \cos(\alpha) a_1 + i \sin(\alpha) a_2, \tag{18a}$$

$$p(\alpha) = \cos(\alpha) p_1 + i \sin(\alpha) p_2, \tag{18b}$$

where a_1, a_2, p_1, and p_2 are complex numbers. Each term in Eq. (10) is the real part of a product of such coefficients, which may be simplified as follows:

$$\begin{aligned}
\mathrm{Re}[p(\alpha)a^*(\alpha)] &= \mathrm{Re}[p_1 a_1^* \cos^2(\alpha) + p_2 a_2^* \sin^2(\alpha) \\
&\quad + i(p_2 a_1^* - p_1 a_2^*)\sin(\alpha)\cos(\alpha)] \\
&= \mathrm{Re}\left(\frac{1}{2}(p_1 a_1^* - p_2 a_2^*)\cos(2\alpha) \right. \\
&\quad \left. + \frac{1}{2}(p_1 a_1^* + p_2 a_2^*) + \frac{i}{2}(p_2 a_1^* - p_1 a_2^*)\sin(2\alpha) \right) \\
&= K_1 + L_1 \sin(2\alpha + \Delta_1),
\end{aligned} \tag{19}$$

$$\begin{aligned}
|p(\alpha)|^2 &= |p_1|^2 \cos^2(\alpha) + |p_2|^2 \sin^2(\alpha) \\
&\quad + i(p_2 p_1^* - p_1 p_2^*)\sin(\alpha)\cos(\alpha) \\
&= \frac{1}{2}(|p_1|^2 - |p_2|^2)\cos(2\alpha) + \frac{1}{2}(|p_1|^2 + |p_2|^2) \\
&\quad + \frac{i}{2}(p_2 p_1^* - p_1 p_2^*)\sin(2\alpha) \\
&= K_2 + L_2 \sin(2\alpha + \Delta_2),
\end{aligned} \tag{20}$$

where the constants K_1, K_2, L_1, L_2, Δ_1, and Δ_2 are functions of the constants a_1, a_2, p_1, and p_2. The torque in Eq. (10) is a sum of many similar terms, each with the same functional dependency. The summation leaves the dependence on α unchanged, allowing the following general relationship between the induced torque and rotation angle to be deduced:

$$\Gamma_z(\alpha) = A + B \sin(2\alpha + \beta), \tag{21}$$

where A, B, and β are constants, independent of α.

Equation (21) corresponds with the form obtained by representing the particle as a point polarizability. However, Eq. (21) is a general result, which may be applied to any extended particle of arbitrary shape in a plane-polarized beam.

The derivation of Eq. (21) is reliant on the restrictions placed on the expansion coefficients of the incident field, which specify that the beam is polarized, i.e., in the present case, that $m=+1$ *and* $m=-1$. These restrictions allow the rotation matrix to be separated into scalar functions of the rotation angle and constant matrices, which forms a crucial part of the analysis. For more general incident fields such a separation would not always be possible and Eq. (21) would contain higher Fourier terms.

One particular case in which Eq. (21) does not apply is that of the circularly polarized trap. In this case we will have either $m=+1$ or $m=-1$. If we take the case $m=+1$, i.e., right-handed circular polarization, the rotation matrix [Eq. (15)] will be $R(\alpha)=\exp(i\alpha)$, yielding

$$\tilde{a}(\alpha) = \exp(i\alpha)\tilde{a}(0), \tag{22a}$$

$$\tilde{p}(\alpha) = \exp(i\alpha) T \tilde{a}(0). \tag{22b}$$

Since all terms in Eq. (10) appear in the form $p_{nm}^{(k)} p_{nm}^{*(k)}$ or $p_{nm}^{(k)} a_{nm}^{*(k)}$, it is clear that the angular dependence will vanish, leaving only the constant A in Eq. (21). Therefore, as observed experimentally, any arbitrarily shaped particle will experience a constant torque when trapped in a circularly polarized beam. In linearly polarized beams, however, the presence of mirror symmetry leads to a relationship between the T-matrix coefficients with $m=+1$ and -1, which results in $A=0$ (see below). Intuitively, one might expect that a circularly polarized beam, being a superposition of two linear polarizations, would also have $A=0$. That this is not the case is a consequence of the fundamental fact that the Maxwell stress tensor is quadratic in the field.

The approach described above neglects the details of the optical interaction completely—they are not required in determining the form given by Eq. (21). However, as already indicated, the symmetry of the particle places constraints on the components of the T matrix, which may be used to make further deductions about the values of the constants A, B, and β. This will be examined further below.

C. *T*-matrix symmetry

The symmetry classification of the particle affects the form of its T matrix which, in turn, dictates the general form of the scattered field coefficients and, thereby, the polarization-induced torque. As far as rotations about the z axis are concerned, the only symmetry operations that play a significant role are those belonging to the two-dimensional point symmetry groups, i.e., rotational transformations about the z axis and reflections in vertical mirror planes. Particles with N-fold rotational symmetry are said to belong to the point group C_N. If, in addition, they have a vertical mirror plane, they belong to the point group D_N. A particle with no particular symmetry is designated C_1, while a particle that has circular symmetry about the z axis belongs to D_∞.

The T matrix may be transformed using the same transformation matrix as the VSWFs and the expansion coefficients. The procedure involved is similar to the coordinate transformations of a second-rank tensor, i.e., premultiplying by the transformation matrix, and postmultiplying by its inverse.

Schulz *et al.* have derived the constraints placed on T matrices by particles with specific symmetries by demanding that the T matrix is invariant under the same transformations as the particle that it represents [31]. For example, if a par-

ticle has N-fold rotational symmetry, the rotation of its T matrix through $2\pi/N$ radians will leave it unchanged, i.e.,

$$R(2\pi/N)TR^{-1}(2\pi/N) = T. \tag{23}$$

If the rotation is about the z axis, then R is the matrix defined in Eq. (15). In terms of individual components this can be written as

$$e^{i2\pi(m-m')/N}T^{(kk')}_{nmn'm'} = T^{(kk')}_{nmn'm'}. \tag{24}$$

Hence, the only nonzero entries of the T matrix of a particle with N-fold rotational symmetry are those for which the exponential part of Eq. (24) is unity. The condition on the elements of the T matrix is therefore given by

$$T^{(kk')}_{nmn'm'} \neq 0 \Rightarrow (m-m') \mod N = 0. \tag{25}$$

The indices m and m' must satisfy the condition in Eq. (25) if the matrix element is nonzero. It is possible for the matrix element to vanish when m and m' satisfy this condition, but this will only happen in special cases and generally Eq. (25) will hold. According to Eq. (24), the demand that the T matrix is left unchanged by a rotation of $2\pi/N$ radians is sufficient to ensure that it is invariant with respect to successive rotations of this sort, provided that the particle possesses N-fold rotational symmetry.

The conditions deriving from the existence of a vertical mirror plane depend on orientation of the plane in question. However, in the present situation, this issue is immaterial. If a particle has N-fold rotational symmetry, then the existence of one mirror plane fixes the symmetry of the particle irrespective of the orientation of the mirror plane considered. Therefore, without loss of generality, any particle with mirror symmetry may be rotated so that it is invariant with respect to reflections in the x-z plane. Reflections of the VSWFs in the x-z plane involve a simple parity rule that results in the following condition on the T matrix given:

$$T^{(kk')}_{n,-mn',-m'} = (-1)^{m+m'}(-1)^{k+k'}T^{(kk')}_{nmn'm'}. \tag{26}$$

The effects of the symmetry conditions on the scattered field coefficients are evident when the matrix multiplications appearing in Eq. (17) are performed explicitly. First, Eq. (17) is rewritten in terms of two new coefficient vectors, $\tilde{\eta}$ and $\tilde{\zeta}$:

$$\tilde{p}(\alpha) = \cos(\alpha)\tilde{\eta} + i\sin(\alpha)\tilde{\zeta}, \tag{27}$$

where

$$\begin{aligned}\eta^{(k)}_{nm} &= \sum_{k'=1}^{2}\sum_{n'=1}^{\infty}\sum_{m'=-n'}^{n'} T^{(kk')}_{nmn'm'}a^{(k')}_{n'm'}(0) \\ &= \sum_{k',n'} T^{(kk')}_{nmn'1}a^{(k^e)}_{n'1}(0) + T^{(kk')}_{nmn',-1}a^{(k')}_{n',-1}(0) \\ &= x^{(k)}_{nm} + y^{(k)}_{nm}\end{aligned} \tag{28}$$

and, similarly,

$$\zeta^{(k)}_{nm} = x^{(k)}_{nm} - y^{(k)}_{nm}. \tag{29}$$

The fact that the incident field coefficients are restricted to those for which $|m|=1$ has been used to simplify the matrix multiplication and subsequently to define another two coefficient vectors, $\tilde{x}$ and $\tilde{y}$, in Eqs. (28) and (29).

For particular symmetries the coefficient vectors $\tilde{x}$ and $\tilde{y}$ (and therefore $\tilde{\eta}$ and $\tilde{\zeta}$) acquire different forms that, on insertion into Eq. (10), give rise to different forms of mechanical behavior. In the case of rotational symmetry, the condition expressed by Eq. (25) results in $T^{(kk')}_{nmn'1}=0$ for all values of k' and n', in which case $x^{(k)}_{nm}$ must also be zero. The condition shown in Eq. (25) may be rewritten as

$$x^{(k)}_{nm} \neq 0 \rightarrow m \in S_1, \quad \text{where} \quad S_1 = \{m : m = Nl+1, l \in \mathbb{Z}\}. \tag{30}$$

A similar condition pertains for the elements of the coefficient vector $\tilde{y}$,

$$y^{(k)}_{nm} \neq 0 \rightarrow m \in S_{-1}, \quad \text{where} \quad S_{-1} = \{m : m = Nl-1, l \in \mathbb{Z}\}. \tag{31}$$

In the following paragraphs the above considerations will be applied to particles with different rotational symmetries. As will be seen, the properties of the sets S_1 and S_{-1} for different values of N are critical in determining the behavior of the system.

The existence of a mirror plane has a different effect on the various coefficient vectors, resulting in parity relations between the components of $\tilde{x}$ and $\tilde{y}$ and, ultimately, between the components of the scattered field coefficients with positive and negative values of m. Using Eq. (26) and the parity properties of the incident field coefficients [Eq. (13)] each component of $\tilde{x}$ can be written as follows:

$$\begin{aligned}x^{(k)}_{nm} &= \sum_{k',n'} T^{(kk')}_{nmn'1}a^{(k')}_{n'1}(0) \\ &= \sum_{k',n'} (-1)^{k+k'}(-1)^{m+1}T^{(kk')}_{n,-mn',-1}(-1)^{k'+1}a^{(k')}_{n',-1}(0) \\ &= (-1)^k(-1)^m y^{(k)}_{n,-m},\end{aligned} \tag{32}$$

or, by putting $m=-m$ into Eq. (32),

$$x^{(k)}_{n,-m} = (-1)^k(-1)^m y^{(k)}_{nm}. \tag{33}$$

Using these relationships in the definitions of $\tilde{\eta}$ and $\tilde{\zeta}$ gives similar relationships between their elements,

$$\eta^{(k)}_{n,-m} = (-1)^k(-1)^m\eta^{(k)}_{nm}, \tag{34a}$$

$$\zeta^{(k)}_{n,-m} = -(-1)^k(-1)^m\zeta^{(k)}_{nm}. \tag{34b}$$

For any particular particle symmetry, the relationships expressed in Eqs. (30), (31), and (34) can be used to derive general expressions for the scattered field coefficients and thence the polarization-induced torque. In the following paragraphs each of the two-dimensional point symmetry groups are considered in turn.

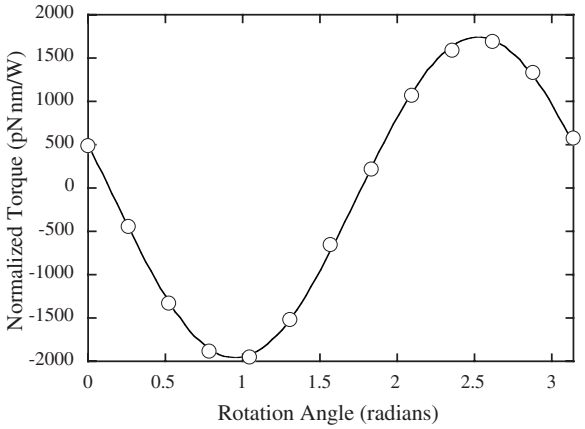

FIG. 4. Normalized torque function for the C_1 particle (open circles) shown in Fig. 2(a), as it is rotated in a plane polarized optical trap. A $\sin(2\alpha)$ fit is also shown (solid line).

1. Symmetry group C_1

For particles that possess no particular two-dimensional symmetry, there are no restrictions on the T matrix and the only significant symmetry, that of the beam, manifests itself through the relationship between the coefficient vectors $\tilde{\eta}$ and $\tilde{\zeta}$ [Eqs. (28) and (29)]. The scattered field coefficients have the following angular dependence:

$$p_{nm}^{(k)}(\alpha) = (x_{nm}^{(k)} + y_{nm}^{(k)})\cos(\alpha) + i(x_{nm}^{(k)} - y_{nm}^{(k)})\sin(\alpha) \quad (35)$$

and they are all, in general, nonzero. Subsets of the scattered field coefficients may disappear if additional symmetries, not included in the definition of the two-dimensional point groups, are present. However, this will not in general affect the polarization-induced torque.

The incident and scattered field coefficients will thus take the general form shown in Eq. (18), and their products will possess the $\sin(2\alpha)$ form of Eqs. (19) and (20). Since the torque, given by Eq. (10), consists of a sum over such products, the angular variation of the torque will be that of Eq. (21), with A, B, and β nonzero in the general case.

The behavior of the system is subsequently dependent on the relative sizes of these constants. If the component of the torque that is independent of rotation angle, given by the parameter A, is larger than the amplitude of the harmonically varying part, B, the particle will undergo continuous rotation. Alternatively, if B is greater than A, equilibrium orientations, for which the induced torque is zero, will appear. The stability of these equilibrium points is given by the sign of the derivative of the torque with respect to α and, because of the form of the torque-angle relationship stable orientations are interleaved with unstable ones.

To confirm and illustrate these observations, FDTD torque calculations have been performed for the irregularly shaped particle shown in Fig. 2(a) and Fig. 3. The calculated torque as a function of rotation angle is shown in Fig. 4, which also shows a fitted $\sin(2\alpha)$ curve. As can be seen the discrepancy between the two is extremely minor and the slightly surprising result, that irregularities in the particle do not give rise to irregularities in the induced torque, is confirmed. In the fit, we find $A=-1.11\times10^2$ pN nm/W, $B=-1.85\times10^3$ pN nm/W, and $\beta=-0.34$ radians. The value of β can be seen to be arbitrary, depending on the initial specification of the particle. B is negative, implying a restoring torque as the long axis of the particle moves away from the polarization direction. The asymmetry in the particle is sufficient to induce a component of torque which is independent of the setting angle of the particle, but not to induce a continuous rotation. The precise values of A and B depend on the choice of rotation center. For computational convenience, this was taken to be the point shown in Fig. 3.

2. Symmetry group D_1

For particles that contain a mirror plane, the torque behavior can be immediately discerned from the symmetry properties of mechanical torque. The torque must vanish whenever the mirror plane of the particle coincides with, or is perpendicular to, the plane containing the beam axis and the polarization direction. Equally, the torque variation must be symmetric about each of the equilibrium orientations. These conditions mean that the angle independent component of the torque [A, in Eq. (21)] must be zero, as will now be shown.

Equation (34) gives the parity relationships that arise between the components of $\tilde{\eta}$ and $\tilde{\zeta}$ for particles containing a mirror plane. Applying these relationships to the scattered field coefficients gives, for $m>0$,

$$p_{nm}^{(k)} = \eta_{nm}^{(k)}\cos(\alpha) + i\zeta_{nm}^{(k)}\sin(\alpha), \quad (36a)$$

$$p_{n,-m}^{(k)} = \eta_{n,-m}^{(k)}\cos(\alpha) + i\zeta_{n,-m}^{(k)}\sin(\alpha) = (-1)^k(-1)^m[\eta_{nm}^{(k)}\cos(\alpha) - i\zeta_{nm}^{(k)}\sin(\alpha)]. \quad (36b)$$

As with the case of C_1 particles, the scattered field coefficients are generally nonzero for all index values. However, when $\alpha=0,\pi,2\pi,\ldots$ they share the parity relationship of the vector coefficients, $\tilde{\eta}$. Similarly, for $\alpha=\pi/2,3\pi/2,\ldots$ they have the same parity as the $\tilde{\zeta}$ coefficients. In either case, the total Poynting vector field has D_1 symmetry, as can be seen by evaluating the field expansions. For example, when $\alpha=0$, the radial component of the scattered electric field is given by

$$E_r = \sum_{n,m}\eta_{nm}^{(2)}\left(\gamma_{nm}\frac{n(n+1)}{|kr|}h_n^{(1)}(kr)P_n^m(\cos(\theta))e^{im\phi}\right) = \sum_n \eta_{n0}^{(2)}\gamma_{n0}\frac{n(n+1)}{|kr|}h_n^{(1)}P_n(\cos(\theta)) + \sum_{n,m>0}\eta_{nm}^{(2)}\gamma_{nm}\frac{n(n+1)}{|kr|}h_n^{(1)}(kr)P_n^m(\cos(\theta))2\cos(m\phi), \quad (37)$$

where the relation

$$\gamma_{nm}P_n^m(\cos(\theta)) = (-1)^m\gamma_{n,-m}P_n^{-m}(\cos(\theta))$$

has been used. The only scattered field coefficients appearing in the above expansion are those for which $k=2$. In these

circumstances Eq. (36) shows that the coefficients for $+m$ and $-m$ are related by $p^{(2)}_{nm}(0)=(-1)^m p^{(2)}_{n,-m}(0)$. It is this property which, in accordance with expectations, causes E_r to be even in ϕ. Similar calculations show that E_t is also even, while E_p changes sign. The reverse is true for the magnetic field resulting in a Poynting vector field that has reflection symmetry in the x-z plane. When $\alpha=\pi/2$, similar considerations lead to the scattered field being symmetric in the y-z plane.

In general the field is, therefore, composed of a linear superposition of two parts, one even with respect to reflections in the x-z plane, the other even with respect to reflection in the y-z plane. As the particle is rotated the scattered field varies between these extreme conditions. As a consequence the torque experienced by the particle varies similarly. This can be seen by using the incident field coefficients [Eq. (12)] together with the scattered fields [Eq. (36)], in Eq. (10). The first part of Eq. (10) consists of a sum over the moduli of the scattered field coefficients. By combining the coefficients with azimuthal index m with those of index $-m$, the contribution of the first part can be written in the following way:

$$\begin{aligned}\Gamma_z^{(1)} &= -\frac{\epsilon_{\text{ext}}}{2\pi k_1^3}\sum_{k,n,m>0} m[|p^{(k)}_{nm}(\alpha)|^2 - |p^{(k)}_{n,-m}(\alpha)|^2] \\ &= -\frac{\epsilon_{\text{ext}}}{2\pi k_1^3}\sum_{k,n,m>0} m[|\eta^{(k)}_{nm}|^2\cos^2(\alpha) \\ &\quad - i(\eta^{(k)}_{nm}\zeta^{*(k)}_{nm} - \zeta^{(k)}_{nm}\eta^{*(k)}_{nm})\sin(\alpha)\cos(\alpha) + |\zeta^{(k)}_{nm}|^2\sin^2(\alpha)] \\ &\quad - m[|\eta^{(k)}_{nm}|^2\cos^2(\alpha) + i(\eta^{(k)}_{nm}\zeta^{*(k)}_{nm} - \zeta^{(k)}_{nm}\eta^{*(k)}_{nm}) \\ &\quad \times\sin(\alpha)\cos(\alpha) + |\zeta^{(k)}_{nm}|^2\sin^2(\alpha)] \\ &= -\frac{\epsilon_{\text{ext}}}{2\pi k_1^3}\sin(2\alpha)\sum_{k,n,m>0} 2m\Im(\eta^{(k)}_{nm}\zeta^{*(k)}_{nm}). \end{aligned} \tag{38}$$

The second part, containing products of scattered and incident field coefficients, contains only terms for which $|m|=1$ and can be written as

$$\begin{aligned}\Gamma_z^{(2)}(\alpha) &= -\frac{\epsilon_{\text{ext}}}{2\pi k_1^3}\text{Re}\left(\sum_{k,n} p^{(k)}_{n1}(\alpha)a^{*(k)}_{n1}(\alpha) - p^{(k)}_{n,-1}(\alpha)a^{*(k)}_{n,-1}(\alpha)\right) \\ &= -\frac{\epsilon_{\text{ext}}}{2\pi k_1^3}\text{Re}\Bigg(\sum_{(k,n)}[\eta^{(k)}_{n1}\cos(\alpha) + i\zeta^{(k)}_{n1}\sin(\alpha)] \\ &\quad \times[a^{*(k)}_{n,1}(0)\cos(\alpha) - ia^{*(k)}_{n,1}(0)\sin(\alpha)] \\ &\quad -[\eta^{(k)}_{n1}\cos(\alpha) - i\zeta^{(k)}_{n1}\sin(\alpha)] \\ &\quad \times[a^{*(k)}_{n,1}(0)\cos(\alpha) + ia^{*(k)}_{n,1}(0)\sin(\alpha)]\Bigg) \\ &= -\frac{\epsilon_{\text{ext}}}{2\pi k_1^3}\sin(2\alpha)\text{Re}\left(\sum_{k,n}(\eta^{(k)}_{n1} + i\zeta^{(k)}_{n1})a^{*(k)}_{n1}(0)\right), \end{aligned} \tag{39}$$

where the parity relations for the incident and scattered field coefficients, Eqs. (12), (13), and (36), have been used. Combining Eqs. (38) and (39) gives a $\sin(2\alpha)$ angular variation for the torque on D_1 particles. There is, however, no angle-independent term, i.e., $A=0$ in Eq. (21). The disappearance of the angle independent term may be seen to be, physically, due to the mirror planes in the beam and particle and, algebraically, as a consequence of the parity of the expansion coefficients of the incident and scattered fields. It may also be noted that the angular offset $\beta=0$, so that the mirror plane of the particle coincides with the plane of polarization of the beam.

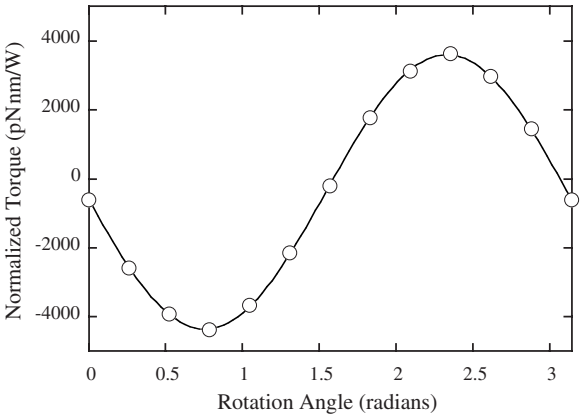

FIG. 5. Normalized torque for a C_2 particle rotating about the beam axis (open circles). The solid line is a $\sin(2\alpha)$ fit.

3. Symmetry group C_2

For rotational symmetry axes, Eqs. (30) and (31) dictate the symmetry implications for the scattered field coefficients. For the dyad axis, $N=2$, it can be seen that the sets S_1 and S_{-1} are both equal to the set of odd integers. Hence, the only nonvanishing components of the scattered field are those for which m is odd. In components, the scattered field coefficients are given by

$$p^{(k)}_{nm}(\alpha) = \begin{cases} (x^{(k)}_{nm} + y^{(k)}_{nm})\cos(\alpha) \\ + i(x^{(k)}_{nm} - y^{(k)}_{nm})\sin(\alpha): & m \text{ odd}, \\ 0: & m \text{ even}. \end{cases} \tag{40}$$

In the absence of a mirror plane, there is no simple relationship between the components of the $\tilde{x}$ and $\tilde{y}$ vector coefficients. The products of scattered and incident field coefficients will be the same as in the C_1 case, and the torque will take the general angular form $A+B\sin(2\alpha+\beta)$. The two systems differ only in the form of the scattered field coefficients. Since the scattered field is given by a sum over terms whose ϕ dependence is given by $e^{im\phi}$, where the index m is always odd, the field components in spherical polar coordinates change sign on rotation through π radians. The same is true for the magnetic field, so that the Poynting vector of the scattered field has twofold rotational symmetry. This is true for all azimuthal orientations of the beam relative to the particle.

FDTD simulations were performed on a two-bladed propeller-shaped particle, similar to the four-bladed version shown in Fig. 2(b). The variation in torque is shown in Fig. 5 together with a fitted $\sin(2\alpha)$ curve. Once again the fit is very close, with parameters $A=-3.88\times10^2$ pN nm/W, $B=-3.98\times10^3$ pN nm/W, and $\beta=0.05$ radians. As expected,

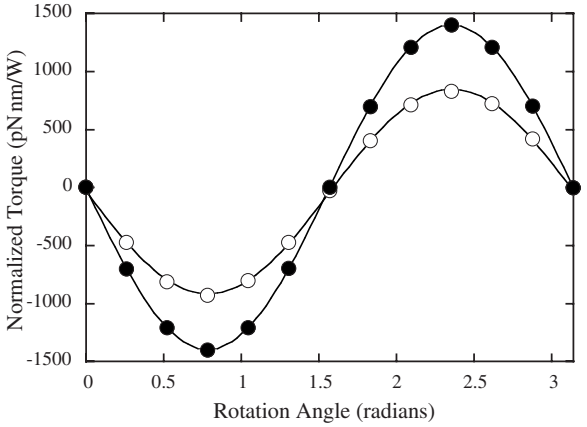

FIG. 6. Normalized torque for a D_2 dumbbell-shaped particle, centered in the beam (solid circles) and displaced so that one end is in the center (open circles). The solid lines are fits to $\sin(2\alpha)$.

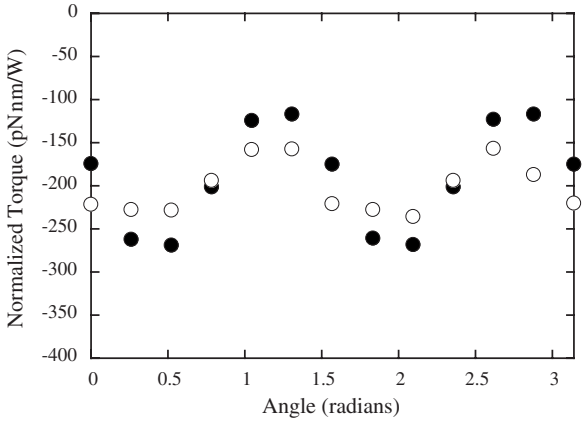

FIG. 7. Normalized torque for a C_4 particle acquired from simulations with lattice spacings of 7 nm (open circles) and 14 nm (solid circles).

the lack of mirror planes through the particle ensures that the constant part of the angular variation, A, need not be zero.

4. Symmetry group D_2

These particles have dyad, or half-turn, symmetry and a vertical mirror plane. As might be expected, their properties are an amalgamation of those of C_2 and D_1 particles. The C_2 symmetry dictates that the only nonzero coefficients in the scattered field expansion are those for which m is odd while the existence of a mirror plane imposes the parity relations that lead to Eq. (36). Hence, the Poynting vector of the scattered field is both even in ϕ (for the orthogonal orientations) and has the half-turn symmetry discussed above. Also as indicated above, the existence of a mirror plane causes the angle-independent contribution to the torque, A, to vanish leaving only the $\sin(2\alpha)$ variation. The mirror symmetry also ensures that β will be zero.

Figure 6 shows the angle-torque relationship for a dumbbell-shaped particle, similar to that shown in Fig. 2(c) but with two arms, as determined by FDTD simulations. Two sets of results are shown. In one case, the particle is centered in the beam, while the second case shows the particle displaced so that it is rotating about one end. It can be seen that the same angular behavior is observed in each configuration, demonstrating that it is the symmetry of the particle, and not the position within the beam, that governs the angular behavior. Also shown are fitted $\sin(2\alpha)$ curves from which it is deduced that both A and β are close to zero, as predicted. In fact, for the centered particle, we observed $|A/B|=0.00001$, whereas for the displaced particle we found $|A/B|=0.04$. This slightly high value for the displaced particle is most likely a consequence of numerical errors in the FDTD simulation, which are less likely to cancel in the lower symmetry case. A more detailed study of numerical errors is presented in the following sections.

5. Symmetry group C_N, $N>2$

The higher order rotational symmetry groups lead to qualitatively different behavior from that of the C_2 particles. For $N>2$, the sets S_1 and S_{-1} are disjoint: if m belongs to S_1 then $m=Nl+1$ for some integer l, but there is no integer, l', for which $m=Nl'-1$, so m does not belong to S_{-1}. Equations (25), (30), and (31) result in the following scattered field coefficients:

$$p_{nm}^{(k)}(\alpha)=\begin{cases} x_{nm}^{(k)}e^{i\alpha}: & m\in S_1, \\ y_{nm}^{(k)}e^{-i\alpha}: & m\in S_{-1}, \\ 0: & \text{otherwise}. \end{cases} \tag{41}$$

For odd values of N the Poynting vector of the scattered field does not have any clear symmetry since the system, comprising the incident field and the particle, is not symmetric irrespective of the particle orientation. When N is even, the Poynting vector of the scattered field has C_2 symmetry, because the underlying system does. In either case, the system never contains a mirror plane, so there is a permanent torque on the particle. Evidently, the modulus of each of the scattered field coefficients is independent of the polarization rotation angle of the beam. Furthermore, since $m=1$ belongs to S_1 and $m=-1$ belongs to S_{-1}, the required products of scattered and incident fields are also independent of angle. The mechanical torque experienced by the particle is therefore independent of orientation, i.e., $B=0$ and the particle will consequently rotate steadily about the beam axis.

FDTD calculations were performed on the four-bladed propeller shown in Fig. 2(c). The results of two sets of calculations are shown in Fig. 7. The open circles show the torque arising when the standard 7 nm grid is used for the calculations. As predicted, there is a dominant constant torque: $A=-201$ pN nm/W in this case. There is no obvious $\sin(2\alpha)$ dependence. However, there appears to be a small $\sin(4\alpha)$ component, with amplitude 39 pN nm/W, which is not expected. To investigate whether this variation, which appears to be linked to the rotational symmetry of the particle, is actually an artifact of the FDTD calculation, a second set of calculations was performed with a grid size of 14 nm (solid circles). With the larger grid, the constant torque component changed slightly to $A=-191$ pN nm/W, whereas the amplitude of $\sin(4\alpha)$ oscillations doubled to 84 pN nm/W.

Therefore, it appears very likely that the behavior observed is arising as a direct result of the coarseness of the grid, and that further grid refinement would reproduce the invariant response that was expected.

6. Symmetry group D_N, $N>2$

Since the D_N groups are formed by adding a mirror plane to the C_N groups, the scattered field coefficients are those of the corresponding C_N group [Eq. (41)], combined with the parity requirements that derive from the mirror plane [Eqs. (32) and (33)], resulting in

$$p_{nm}^{(k)}(\alpha)=\begin{cases} x_{nm}^{(k)}e^{i\alpha}: & m\in S_1, \\ (-1)^k(-1)^m x_{n,-m}^{(k)}e^{-i\alpha}: & m\in S_{-1}, \\ 0: & \text{otherwise}. \end{cases} \tag{42}$$

In addition, S_1 and S_{-1} are such that, if m belongs to S_1, $-m$ belongs to S_{-1}, as can be discerned from the definitions of the sets. Consequently, if m belongs to S_1 and $p_{nm}^{(k)}=x_{nm}^{(k)}e^{i\alpha}$ then $p_{n,-m}^{(k)}=(-1)^k(-1)^m x_{nm}^{(k)}e^{-i\alpha}$. As seen previously, the presence of a mirror plane in the particle gives rise to a mirror plane in the Poynting vector of the scattered field. In the case of the particle with D_1 symmetry it was necessary for the symmetry plane of the particle to coincide with that of the incident Poynting vector field, for the torque to vanish. This is not necessary here: the Poynting vector of the scattered field is symmetric whatever the orientation of the particle so the torque is always zero. This can be seen algebraically from Eq. (42). Evidently the moduli of the scattered coefficients are independent of α. In fact $|p_{nm}^{(k)}|=|p_{n,-m}^{(k)}|$ so that the first part of Eq. (10) vanishes. The second part cancels out in a similar way, so that $\Gamma_z^{(1)}$ and $\Gamma_z^{(2)}$ are each separately equal to zero.

Figure 8 shows FDTD results acquired for particles with D_3 and D_4 symmetry. In both cases, there is no constant term, i.e., $A=0$, but small-amplitude oscillations are evident, with period related to the particle symmetry, i.e., $\sin(3\alpha)$ for the D_3 particle and $\sin(4\alpha)$ for the D_4 particle. For the D_3 case, three sets of data are given, relating to simulations using successively finer lattices. It is clear that the oscillation amplitude diminishes as the lattice becomes finer, and converges on the anticipated zero result.

D. Other beams

From the above analysis it can be seen that there are two principal forms of behavior. Particles for which C_N is a symmetry operation, for $N\leqslant 2$, are sensitive to orientation while for $N>2$, they are not. The algebraic cause for this lies in the fact that for the beams dealt with above, the sets S_1 and S_{-1} are identical when $N\leqslant 2$, and disjoint when $N>2$. When S_1 and S_{-1} are disjoint the scattered field coefficients are of the form $ce^{i\alpha}$, for complex c, so that their moduli are independent of orientation. When they are identical, the scattered field coefficients are of the general form $be^{i\alpha}+ce^{-i\alpha}$ so that the moduli vary with α.

The conditions under which S_1 and S_{-1} are distinct or identical, and thereby the conditions under which the trap is rotationally sensitive, can be altered by extending the discussion to higher order beams. The set of expansion coefficients given in Eq. (43) relate to a hollow beam that on symmetry grounds does not carry angular momentum and is linearly polarized:

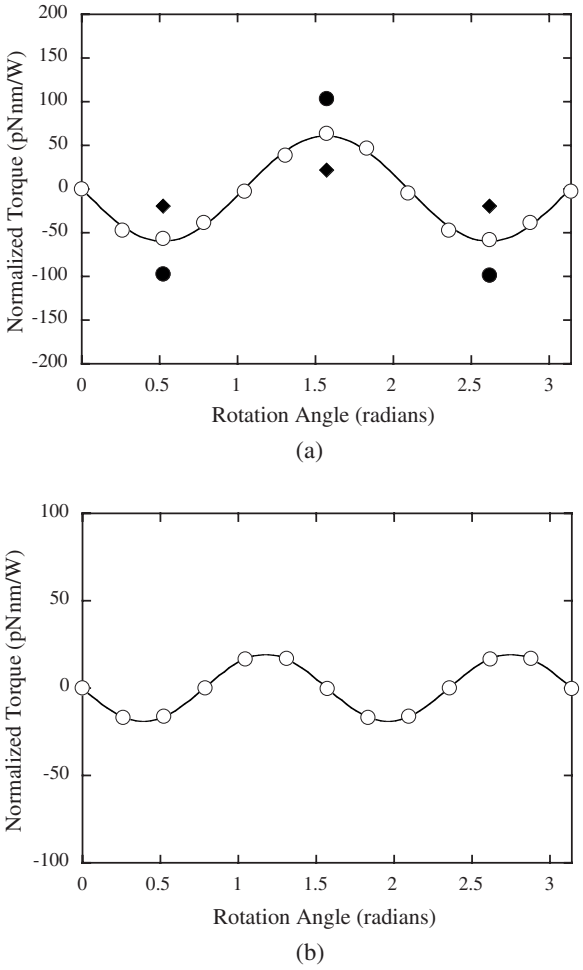

FIG. 8. (a) Normalized torque for a D_3 particle acquired from FDTD simulations with lattice spacings of 7 nm (open circles), 14 nm (solid circles), and 3.5 nm (diamonds). The solid line is a fit to $\sin(3\alpha)$. (b) Normalized torque for a D_4 particle with lattice spacing 7 nm. The solid line is a fit to $\sin(4\alpha)$.

$$a_{nm}^{(k)}=\begin{cases} (\mathrm{sgn}(m))^{k+1}g_n: & |m|=L, \\ 0: & \text{otherwise}. \end{cases} \tag{43}$$

Here, L is the order of the beam. The rotation matrix in Eq. (15) becomes

$$R(\alpha)=\cos(L\alpha)I_1+i\sin(L\alpha)I_2, \tag{44}$$

and the generalized torque expression, Eq. (21), is rewritten as

$$\Gamma_z(\alpha)=A+B\sin(2L\alpha+\beta). \tag{45}$$

The sets S_1 and S_{-1} are redefined as follows:

$$S_L=\{m: m=Na-L, a\in\mathbb{Z}\}, \tag{46a}$$

$$S_{-L} = \{m : m = Na + L, a \in \mathbb{Z}\}. \quad (46b)$$

These sets are identical when $2L \bmod N = 0$, and disjoint otherwise. For example, a beam of this type, with $L=3$, would be sensitive to the orientation of particles with twofold and threefold rotational symmetry. If in addition the particle contained a vertical mirror plane and belonged to the two-dimensional group, D_3, it would have a preferred orientation in the beam and could therefore be rotated at will. Although these beams look unusual it can be shown that an example of an L-order beam is provided by the superposition of two circularly polarized Laguerre-Gaussian beams, one of order L and with circular polarization in one sense and the other of order $-L$ with circular polarization in the opposite sense. As a consequence they can be easily generated by a holographic optical tweezer and would find practical application, for example, in the manipulation of higher symmetry particles for the purposes of microassembly.

IV. DISCUSSION

In the preceding pages we have presented a thorough analysis of the phenomenon of polarization-induced torque. The general relationship between torque and orientation angle is $\Gamma = A + B\sin(2\alpha + \beta)$. The assumptions made in reaching this relationship are minimal. That a linear relationship should exist between the scattered and incident field expansion coefficients is not formally restrictive, although there are technical difficulties in evaluating transition matrices for certain sorts of particles. The existence of a T matrix is a consequence of the linearity of Maxwell's equations and therefore depends only on the linearity of the optical properties of the materials involved. In addition, nothing has been assumed about the size, shape, or composition of the particle and the general form of the angular variations can be seen as a consequence of the rotational properties of the incident field.

For any particular beam, the behavior of the particle in the beam is dictated by its two-dimensional point symmetry group. There are four qualitatively distinct forms of behavior that can be summarized as follows:

(1) $|A| > 0$, $|B| > 0$: This is the general case, occurring when the system has low symmetry and no mirror planes, i.e., C_1 and C_2.

(2) $A=0$, $|B| > 0$: This situation occurs for particles with symmetry D_1 and D_2. There are two stable equilibrium orientations, separated by π radians, with unstable equilibria halfway in between.

(3) $|A| > 0$, $B=0$: This is relevant for chiral particles belonging to C_N with $N > 2$. The result is uniform rotation in the beam.

(4) $A=B=0$: This is a result for particles with D_N symmetry (including spheres), with $N > 2$. Polarization-induced torque is completely absent.

For higher order beams consisting, for example, of counter-rotating circularly polarized Laguerre-Gaussian beams analogous behavior is observed, but the dependence on particle symmetry is modified. An order 3 beam, of the type discussed above, can orient a particle belonging to D_3, for instance.

In reaching the above conclusions, general forms for the scattered fields have been exhibited. A salient feature, in each case, is the presence in the scattered beam of VSWFs with azimuthal indices, m, with magnitudes greater than one. These VSWFs are hollow, in that they have zero amplitude on the z axis. In other words they contain a phase singularity around which the field varies with azimuthal dependence $e^{im\phi}$. Because of these properties, a beam consisting of VSWFs of fixed m, with $|m| > 1$ would be associated with orbital, as well as spin, angular momentum [32]. The scattered field consists of a superposition of beams of this sort and, as such, one would expect it to be carrying orbital angular momentum. Unfortunately these matters are difficult to quantify; Barnett, for example, was unable to find a physically meaningful way of separating spin from orbital angular momentum for a dipole, let alone a multipole expansion [33]. Nevertheless, the complicated azimuthal dependence of the scattered field indicates that the momentum coupling occurring as a result of scattering is more involved than a simple exchange of spin angular momentum.

Experimental results are available for some, but not all, of the above cases. The simplest case studies consist of glass cylinders, constrained to lie perpendicular to the beam axis by the presence of a microscope slide. Such rods possess D_2 symmetry, and have been demonstrated to follow the $\sin(2\alpha)$ torque law derived above [11,12]. Equally, it has been shown that discs oriented perpendicular to the beam, i.e., D_∞ particles, do not experience any torque about that axis [34]. Galajda and Ormos have presented results from a range of particles with different symmetries [1,30,35]. In some experiments they have used particles with long stalks parallel to the symmetry axis that preferentially take up the required orientation in the beam. Thus, D_2 particles created in this manner have displayed the $\sin(2\alpha)$ behavior [1], while various 3D propeller structures with C_N symmetry have been used to demonstrate continuous rotation [35]. In yet other experiments, flat particles with C_5 symmetry have been shown to vary their rotation direction depending on their position in the beam, i.e., whether they are above or below the focus [30].

The predictions discussed above have been accompanied by numerical simulations demonstrating the various special cases. The simulations have a dual purpose: they serve to confirm the underlying theory and simultaneously to characterize the accuracy of FDTD based calculations of this sort. FDTD simulations are beginning to find applications in optical trapping [22–24], so it is helpful to have an assessment of their reliability. The agreement between the simple theoretical expression, modified by symmetry considerations, has been seen to be strong in most instances. Where discrepancies arise, they can be seen to reduce in magnitude as the simulation lattice is refined suggesting that they are the result of numerical error.

The most obvious deviations from the predicted behavior appear to take the form of residual oscillations in the torque versus angle graphs. This observation can be simply interpreted. For example, the D_3 particle, for which the expected torque was uniformly zero, can be thought of as a superposition of three displaced D_2 particles each of which would have a $\sin(2\alpha)$ dependence on the torque. If optical interac-

tions between these constituent particles are assumed to be negligible, then the torque on the whole object is given by the sum of the torques on its parts:

$$\Gamma_z(\alpha) = \text{const} \times \sin(2\alpha) + \sin(2\alpha - 2\pi/3) + \sin(2\alpha + 2\pi/3) = 0.$$

In order to replicate this result, a similar cancellation effect has to take place within the simulation. However, in the simulation, a complex shape is being represented on a cubic lattice, and it is inevitable that the coarseness of the lattice will influence how precisely the cancellation can occur. An inspection of the magnitudes of these residual oscillations show that this cancellation is achieved to a great extent. For the D_3 particle on a 7 nm lattice, the residual $\sin(3\alpha)$ oscillations are smaller by a factor of ~ 25 than the $\sin(2\alpha)$ variation predicted for the D_2 particle. It is clear from these results that accurate answers are always available from FDTD simulations, given sufficient time and computer power, and that care should always be taken to refine the lattice size to ensure that the trapped particles are adequately represented.

Experimental and theoretical work on the higher symmetry particles discussed here, e.g., D_N where $N>2$, does not exist in the literature, possibly due to a lack of obvious applications. The freedom of rotation for such particles does, however, offer a simple system for allowing the observation of rotational Brownian motion. Alternatively, since the lack of restricting torque is dependent on the symmetry of the system, such particles would be sensitive to small perturbations in their environment and could hence be used to create a rotational variant of the photonic force microscope.

Potential avenues for theoretical research also present themselves. When calculating an angular momentum flux, a question arises as to its decomposition into spin and orbital components, the former being associated with polarization, the latter with spatial variation. Under the paraxial approximation this separation is meaningful and unambiguous [32]. Beyond this approximation the situation becomes more complicated. This is partly because, in the absence of the paraxial approximation, the electric field vector will describe an ellipse whose size, orientation, and eccentricity vary from point to point. As a consequence it becomes difficult to identify a portion of the angular momentum flux as being associated exclusively with the polarization state of the field. As observed in Ref. [33] beyond the paraxial approximation, the distinction between spin and orbital angular momentum is problematic in all but the simplest of geometries. In the systems studied here, the incident field is linearly polarized (in the sense that the aforementioned ellipses are vertically oriented), and therefore does not carry angular momentum of either variety. The total field surrounding the scattering particle does, in general, carry angular momentum although, for the reasons outlined above, it is difficult to disentangle the spin and orbital contributions. However, as has been shown, the azimuthal variation of the scattered fields generally contains higher order Fourier components which, by analogy with the well-known Laguerre-Gaussian beams (see [32], for example), suggest that the angular momentum flux is not exclusively of the spin variety. This is a matter for further analysis.

V. CONCLUSIONS

We have demonstrated, through an application of T-matrix theory, that the polarization-induced torque on a nonspherical particle in an optical trap takes the general form $\Gamma_z = A + B\sin(2\alpha+\beta)$, in which A, B, and β are constants dependent on the symmetry of the system, and α is the angle between the principal axis of the particle and the polarization vector. The result applies equally to any extended dielectric particle of arbitrary shape. The only assumption is the existence of a T-matrix for the particle, which is guaranteed by the linearity of Maxwell's equations.

If the particle contains a single vertical mirror plane then the constant A becomes zero, and the particle orients itself within the beam, so that the mirror plane coincides with the plane of polarization. If the particle has N-fold rotational symmetry, where $N \geqslant 3$, the constant B vanishes and the particle will rotate steadily. If both symmetry operations are present, i.e., a D_N symmetry with $N \geqslant 3$, the particle will not feel a torque. The predictions have been confirmed through the use of FDTD numerical simulations, and are consistent with a range of literature reports.

For higher order beams consisting, for example, of counter-rotating circularly polarized Laguerre-Gaussian beams analogous behavior is observed, but the dependence on particle symmetry is modified. For example, an order 3 beam, of this type, can orient a particle with D_3 symmetry, which cannot be oriented by a plane-polarized beam.

ACKNOWLEDGMENTS

The authors wish to thank Stephen Barnett and Miles Padgett for helpful discussions. The authors are grateful to the United Kingdom Research Councils (RCUK) for financial support from the Basic Technology programme.

APPENDIX: ROTATION THEOREM FOR VSWFs

The rotation theorem for VSWFs is given by

$$\mathbf{M}_{nm}(kr,\theta_2,\phi_2) = \sum_{m'=-n}^{n} \mathbf{M}_{nm'}(kr,\theta_1,\phi_1) D^n_{m'm}(\alpha,\beta,\gamma), \tag{A1}$$

$$\mathcal{R}\mathbf{M}_{nm}(kr,\theta_2,\phi_2) = \sum_{m'=-n}^{n} \mathcal{R}\mathbf{M}_{nm'}(kr,\theta_1,\phi_1) D^n_{m'm}(\alpha,\beta,\gamma), \tag{A2}$$

where $D^n_{m'm}(\alpha,\beta,\gamma) = e^{-im'\alpha} d^n_{m'm}(\beta) e^{-im\gamma}$ are the Wigner D functions and $d^n_{m'm}$ are Wigner d functions. Rotations of $\mathbf{N}_{nm}$

and $\mathcal{R}\mathbf{N}_{nm}$ follow a similar rule. α, β, and γ are the Euler angles describing the rotation. For rotations about the z axis, β and γ are zero and $d^n_{m'm}(0)=\delta_{mm'}$ so that for $\mathbf{M}_{nm}$ the rotation rule becomes

$$\mathbf{M}_{nm}(kr,\theta_2,\phi_2)=e^{-im\alpha}\mathbf{M}_{nm'}(kr,\theta_1,\phi_1), \tag{A3}$$

and similarly for the other VSWFs. Equivalently, the rotation matrix, R in Eq. (14), is diagonal with entries given by $e^{im\alpha}$.

[1] P. Galajda and P. Ormos, Opt. Express **11**, 446 (2003).
[2] A. Mukhopadhyay and S. Granick, Curr. Opin. Colloid Interface Sci. **6**, 423 (2001).
[3] T. Strick, J.-F. Allemand, V. Croquette, and D. Bensimon, Prog. Biophys. Mol. Biol. **74**, 115 (2000).
[4] L. Oroszi, P. Galajda, H. Kirei, S. Bottka, and P. Ormos, Phys. Rev. Lett. **97**, 058301 (2006).
[5] W. A. Shelton, K. D. Bonin, and T. G. Walker, Phys. Rev. E **71**, 036204 (2005).
[6] J. P. Barton, D. R. Alexander, and S. A. Schaub, J. Appl. Phys. **66**, 4594 (1989).
[7] J.-S. Kim and S.-W. Kim, Appl. Opt. **39**, 4327 (2000).
[8] T. A. Nieminen, H. Rubinsztein-Dunlop, and N. R. Heckenberg, J. Quant. Spectrosc. Radiat. Transf. **70**, 627 (2001).
[9] T. A. Nieminen, H. Rubinsztein-Dunlop, N. R. Heckenberg, and A. I. Bishop, Comput. Phys. Commun. **142**, 468 (2001).
[10] R. C. Gauthier, Appl. Opt. **40**, 1961 (2001).
[11] K. D. Bonin, B. Kourmanov, and T. G. Walker, Opt. Express **10**, 984 (2002).
[12] A. I. Bishop, T. A. Nieminen, N. R. Heckenberg, and H. Rubinsztein-Dunlop, Phys. Rev. A **68**, 033802 (2003).
[13] A. La Porta and M. D. Wang, Phys. Rev. Lett. **92**, 190801 (2004).
[14] C. Rockstuhl and H. P. Herzig, J. Opt. Soc. Am. A **22**, 109 (2005).
[15] S. H. Simpson and S. Hanna, J. Opt. Soc. Am. A **24**, 430 (2007).
[16] M. I. Mishchenko, L. D. Travis, and A. A. Lacis, *Scattering, Absorption and Emission of Light by Small Particles* (Cambridge University Press, Cambridge, 2002); available online at http://www.giss.nasa.gov/~crmim/books.html
[17] S. H. Simpson and S. Hanna, J. Opt. Soc. Am. A **23**, 1419 (2006).
[18] P. C. Waterman, Phys. Rev. D **3**, 825 (1971).
[19] P. M. Morse and H. Feshbach, *Methods of Theoretical Physics* (McGraw-Hill, New York, 1953), pp. 1865 and 1866.
[20] A. Taflove, *Computational Electrodynamics: The Finite-Difference Time-Domain Method* (Artech House, Boston, 1995).
[21] *Advances in Computational Electrodynamics: The Finite-Difference Time-Domain Method*, edited by A. Taflove (Artech House, Boston, 1998).
[22] A. D. White, Comput. Phys. Commun. **128**, 558 (2000).
[23] J. L. Deng, Q. Wei, and Y. Z. Wang, Opt. Express **13**, 3673 (2005).
[24] R. C. Gauthier, Opt. Express **13**, 3707 (2005).
[25] S. D. Gedney, IEEE Trans. Antennas Propag. **44**, 1630 (1996).
[26] S. A. Schelkunoff, Commun. Pure Appl. Math. **4**, 43 (1951).
[27] M. Lax, W. H. Louisell, and W. B. McKnight, Phys. Rev. A **11**, 1365 (1975).
[28] O. Moine and B. Stout, J. Opt. Soc. Am. B **22**, 1620 (2005).
[29] A. Ashkin and J. M. Dziedzic, Science **235**, 1517 (1987).
[30] P. Galajda and P. Ormos, Appl. Phys. Lett. **80**, 4653 (2002).
[31] F. M. Schulz, K. Stamnes, and J. J. Stamnes, J. Opt. Soc. Am. A **16**, 853 (1999).
[32] L. Allen, M. W. Beijersbergen, R. J. C. Spreeuw, and J. P. Woerdman, Phys. Rev. A **45**, 8185 (1992).
[33] S. M. Barnett, J. Opt. B: Quantum Semiclassical Opt. **4**, S7 (2002).
[34] Z. Cheng, P. M. Chaikin, and T. G. Mason, Phys. Rev. Lett. **89**, 108303 (2002).
[35] P. Galajda and P. Ormos, J. Opt. B: Quantum Semiclassical Opt. **4**, S78 (2002).